Effects of heater surface orientation on the critical heat flux—I. An experimental evaluation of models for subcooled pool boiling

MATTHEW J. BRUSSTAR

Stirling Thermal Motors, Inc., 275 Metty Drive, Ann Arbor, MI 48103-9444, U.S.A.

and

HERMAN MERTE, JR, ROBERT B. KELLER and BRIAN J. KIRBY

The University of Michigan, Department of Mechanical Engineering and Applied Mechanics,
2250 G. G. Brown Laboratory, Ann Arbor, MI 48109-2125, U.S.A.

Abstract—An experimental study of boiling at high heat fluxes in low-velocity subcooled forced convection boiling is presented, demonstrating the effects of subcooling and buoyancy orientation on the critical heat flux (CHF) and the bubble residence time. At the low velocity of 0.04 m s^{-1} used, the flow forces acting on the vapor are insignificant compared with buoyancy and the CHF behaves as in pool boiling, depending primarily on the orientation of the heater surface with respect to gravity. This dependence is related to the bubble residence time, which is found to be inversely proportional to the CHF for all heater orientations at a given operating condition. This relationship, that the product of the CHF and the corresponding bubble residence time is a constant, suggests that the mechanism for dryout is independent of the heater surface orientation, despite changes in the vapor departure velocity and the CHF with the orientation angle. Furthermore, increases in the bulk liquid subcooling substantially reduce the net rate of vapor generation such that the bubble residence times at the CHF are independent of subcooling. The work concludes by proposing the energy per unit area leaving the heater surface during the bubble residence time as the CHF mechanism, which is more generalized than the mechanism assumed in the macrolayer dryout models. © 1997 Elsevier Science Ltd.

INTRODUCTION

The adequacy of existing pool boiling critical heat flux (CHF) models has been found to be somewhat limited, particularly with regard to their ability to correlate certain secondary variables applied in the laboratory. The two most prominent models are the macrolayer dryout models [1, 2] and the hydrodynamic instability models [3, 4]. The former suggests a two-step mechanism for the CHF, in which a thin liquid layer is vaporized during the transient growth and departure time of an overlying vapor mass. Models of this type appear to have supplemented the earlier hydrodynamic instability models, which assume a mechanism in which the vapor escape passages suddenly collapse, due to a capillary instability between the vapor and liquid phases. Both types of models share common dimensional groups and, not coincidentally, also predict the same value for the CHF in saturated pool boiling, since certain empirical factors in the macrolayer dryout model are evaluated using the CHF prediction of Zuber [3] as a reference value. These models have been successful in predicting the CHF for many different fluids, owing to a certain extent to their physically

accurate characterization of the actual boiling phenomenon at CHF. Furthermore, the macrolayer dryout models, including the more recent vapor stem models [5], have provided a useful structure within which many semi-empirical relations can be incorporated. Despite this, such models remain physically inconsistent with some commonly observed phenomena, which inhibit more universal applications where factors such as heater surface character and orientation relative to gravity, for example, may be significant. Additionally, the hydrodynamic models, while successful at identifying dimensional groups germane to the CHF in pool boiling, are based upon a premise of an interfacial instability which has never been observed in practice. The purpose of the current work here is to identify certain strengths and weaknesses of existing models of the CHF in pool boiling, and to provide measurements and high-speed photographs to ascertain their validity in describing various aspects of boiling at high heat fluxes.

The foundations of current CHF models lie mostly in earlier experimental works. Kirby and Westwater [6] and Katto and Yokoya [7] identified the pre-eminence of large bubbles at high heat fluxes by means of high speed photographs of pool boiling. Accordingly,

NOMENCLATURE

a	upper threshold on the indicator function		x	measured axial distance from the leading edge of the heater surface [m]
A	area [m^2]			
b	lower threshold on the indicator function		y	measured normal distance from the heater surface [m].
c	virtual mass coefficient			
c_{pl}	specific heat of the liquid phase [kJ kg^{-1} K^{-1}]		**Greek symbols**	
			$\bar{\alpha}$	mean void fraction [%]
E''	product of CHF and bubble residence time [kJ m^{-2}]		δ	bubble boundary layer thickness [m]
$\bar{f}$	mean bubble frequency [s^{-1}]		ϕ	latent heat fraction, equation (5)
g	gravitational acceleration [m s^{-2}]		ϕ'	latent heat fraction corrected for subcooling, equation (6)
h_{fg}	latent heat of evaporation [kJ kg^{-1}]		θ	orientation angle as designated in Fig. 3 [degrees]
Ja	Jakob number ($= \rho_l c_{pl} \Delta T_{sub}/\rho_v h_{fg}$)			
L	heater length [m]		ρ	density [kg m^{-3}]
q_c	CHF [kW m^{-2}]		σ	surface tension [kg s^{-2}]
q_{co}	q_z corrected for subcooling [equation (1)] [kW m^{-2}]		τ, τ_{res}	bubble residence time [s].
q_s	surface heat flux [kW m^{-2}]		**Subscripts**	
q_z	CHF in saturated pool boiling predicted by Zuber's model [equation (2)] [kW m^{-2}]		c	CHF
			BBL	bubble boundary layer
			v	vapor
Re	Reynolds number based on hydraulic diameter		l	liquid
			local	local temporal average
T_{in}	bulk temperature measured at the inlet to the test section		xyt	spatio-temporal average
			s	surface
ΔT_{sub}	bulk liquid subcooling [K]		o	horizontal, facing-upward orientation.
U	velocity [m s^{-1}]			
v'	volumetric rate of vapor generation [m^3 s^{-1}]		**Superscripts**	
			*	at departure.

Haramura and Katto [1] and, more recently, Kumada and Sakashita [8] formulated macrolayer dryout models considering only the growth and motion of large bubbles. The macrolayer dryout models also identify the primary importance of thin film evaporation, observed earlier, for example, in the photographs of Kirby and Westwater [6] taken from beneath the boiling surface at heat flux levels approaching the CHF. The assumption of a macrolayer, however, implies the existence of a more-or-less uniform liquid layer on the surface, which appears physically untenable except possibly as a first approximation. The vapor stem model described by Liaw and Dhir [5] improves the accuracy of such a model, but remains constrained by some of the inaccurate assumptions associated with the macrolayer, as will be elaborated upon below. The origin and physical basis of the macrolayer and vapor stem models lie primarily in the photographic study of pool boiling by Gaertner [9]. A reconsideration of this work, however, suggests some leeway for alternative interpretations, exclusive of the conjectural concepts of vapor stems and macrolayers first introduced there. The experiments in the present work are intended to assess the viability of these concepts,

whose physics have been incorporated in the vapor stem and macrolayer models, and will also present some evidence by which to judge the validity of the hydrodynamic instability models. The ultimate goal is to provide additional insight, by means of which a more physically accurate model of the CHF can be constructed with more universal applicability than earlier models.

The present work addresses many of the key areas of the existing CHF models for pool boiling, including bubble dynamics, the mechanisms for evaporation and the effect of subcooling. These are examined, experimentally, by varying the bulk liquid subcooling and orientation of the heater surface relative to gravity, which alters the rate of vapor removal as well as the CHF. At the same time, a common mechanism for evaporation and dryout is observed for all orientations and subcoolings. Using a copper heater surface to measure the CHF and hot wire anemometry to measure the void fraction distribution and bubble frequency, a mechanism for the CHF is inferred that is, in many respects, similar to those expounded in previous works. A quantity of energy per unit area is proposed as a more generalized description of the
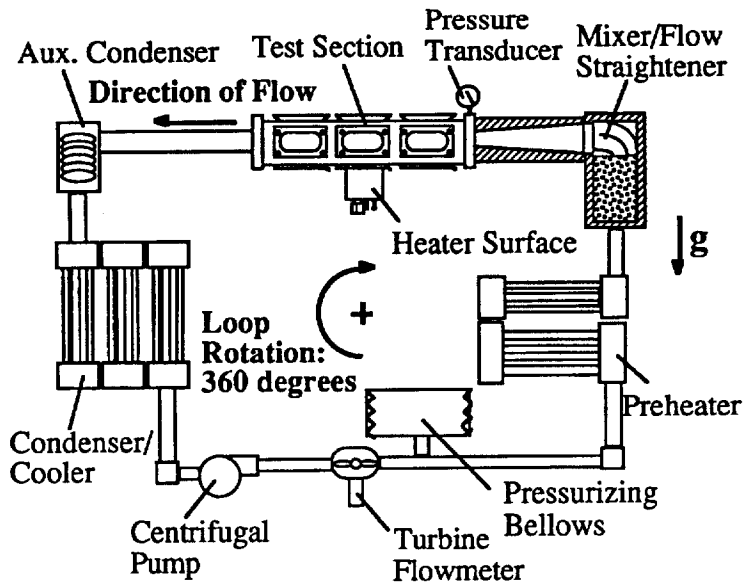
Fig. 1. Schematic of the forced convection boiling loop.

macrolayer thickness, which implies no uniform thin liquid film structure, but otherwise remains consistent with the basic assumptions of the macrolayer dryout model. Finally, high-speed photographs of boiling at high heat flux levels are presented, which give a visual picture of the characteristics of the vapor bubbles as well as the thin film regions on the heater surface.

EXPERIMENTAL APPARATUS

A brief description of the experimental apparatus is given below. Further details may be found in an earlier work [10].

Forced convection boiling loop

The boiling experiments were conducted in a forced convection loop, shown schematically in Fig. 1, with R113, degassed and purified through special filtering and distillation procedures. The system provides for the control of the bulk liquid temperature and subcooling at the test section inlet and the orientation of the heater surface with respect to gravity. The flow velocity in the test section is maintained constant here at 0.04 m s^{-1}, giving conditions very close to those in pool boiling. The entire loop can be rotated about its center of gravity, as shown, and fixed at any orientation between 0 and 360°. The salient features of the loop are summarized below.

The flow rate through the test section can be set within ±2% of the desired level, while the pressure in the loop is maintained within about ±0.17 kPa of its set point by means of a pneumatically-controlled stainless steel bellows. At the same time, the temperature of the fluid at the inlet to the test section is controlled to within about ±0.12 K about the operating temperature of 322 K, using two heat exchangers following the pump exit. The pressure set point is adjusted to provide the desired level of subcooling in the test section for the prescribed liquid temperature, giving a total uncertainty in the subcooling of ±0.2 K.

The test section is shown in detail in Fig. 2 and consists of a rectangular duct, 105 mm wide by 12.7 mm high by 356 mm long. On the sides, and opposite the test surface, are optical-grade quartz windows which allow for transverse as well as overhead views of the heater surface during operation. The heater consists of a copper block heated by three cartridge heaters in its base. The heater surface is 19.1 mm long by 38.1 mm wide and is flat so as to maintain a constant orientation between the buoyancy force and the heater surface. The heater was first operated in air prior to installation in the flow loop to calibrate the heat loss to the surroundings as a function of the base temperature of the heater. The mean surface heat flux, at the CHF and otherwise, was determined by dividing the difference of the power input to the heater and the estimated peripheral heat losses by the heater surface area.

The heater surface used for the photographic study consisted of a thin, semi-transparent gold film sputtered on a quartz substrate. Using a Kodak Ektapro high-speed camera and diffuse backlighting, photographs of boiling looking through the heater surface from below were acquired at a rate of 500 frames per s.

A hot wire probe was chosen among other instrumentation devices for measuring the void fraction and bubble frequency, as it is a reasonably straightforward and economical means of obtaining such measurements with ample bandwidth and signal-to-noise characteristics. The hot wire probe consisted of a platinum sensing wire, 0.025 mm in diameter by 1.3 mm in length, across which a constant current was applied
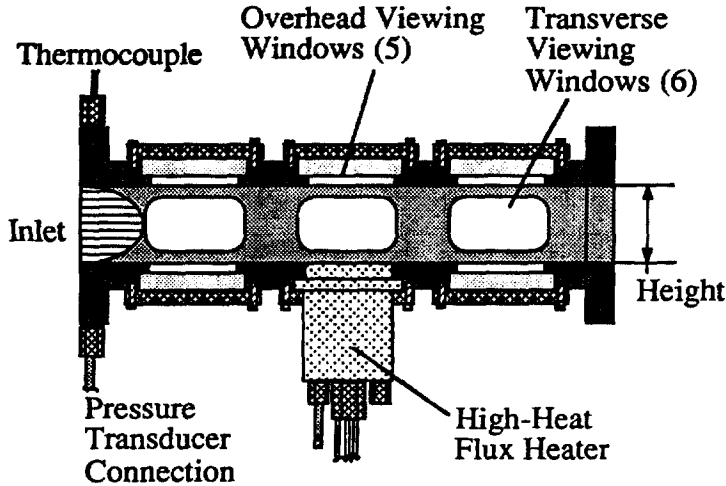
Fig. 2. Illustration of the test section.

such that small changes in the wire resistance would produce an appreciable difference in voltage to distinguish the presence of liquid vapor at the probe tip. A specially-designed displacement mechanism provided a means of accurately moving the probe in two orthogonal directions, one normal to the heater surface and the other in the direction of flow. The probe displacements were measured by two dial indicators, each with a range of 25.4 mm, marked in increments of 0.025 mm (0.001 in).

EXPERIMENTAL PROCEDURES

The experiments were conducted by first setting the orientation, flow velocity, pressure and temperature in the test section to the desired values and allowing sufficient time for the system to reach steady operating conditions. Once quasi-steady nucleate boiling had been initiated on the heater surface, the voltage was raised incrementally, allowing the surface to reach a quasi-steady temperature at each step. When a sudden rise in the surface temperature was observed following an incremental increase in the heater power, the transition to film boiling was assumed to have occurred and the last recorded steady-state operating condition was used to calculate the CHF. The uncertainty in the CHF so measured was estimated to be ± 15 kW m^{-2}, and all measurements were reproducible within this uncertainty. This uncertainty also applies to the horizontal, downward-facing orientation, although the temperature excursions accompanying the extraordinarily low levels of heat flux at dryout for this orientation were rather modest and, consequently, difficult to discern.

The various orientations used are defined with respect to the horizontal upward position in Fig. 3, with the fluid flow directions over the heater surface as indicated by the arrows. Orientations intermediate to those shown are defined by counterclockwise rotation, thus the vertical upflow corresponds to

$\theta = 90°$, the horizontal facing downward to $\theta = 180°$ and the vertical downflow to $\theta = 270°$.

Hot wire data reduction and uncertainty estimate

The signal processing steps used to calculate the bubble frequency and void fraction from the raw hot wire signals are shown in the flowchart in Fig. 4. The raw signal is first sent through a 1000 Hz analog prefilter, then sampled at 400 Hz for approximately 30 s, which was suitably fast to capture all of the relevant dynamic features of each individual event and long enough to ensure ergodicity. The mean, or peak bubble frequency is determined by a spectral analysis of the data record followed by a weighted average, using the power spectral density as the weighting function. The peak bubble frequency measured as such was significantly lower than the measured bandwidth of the hot wire sensor, estimated to be a minimum of 60 Hz. The local void fraction, meanwhile, is determined by first differentiating the data with respect to time to identify the high rates of change in the signal associated with the intercepting of the vapor–liquid interface. Next, the upper and lower trigger levels are set on the derivative signal, from which an indicator function signal is then generated, with a '1' assigned to the presence of vapor and a '0' assigned to the presence of liquid. The local void fraction is then
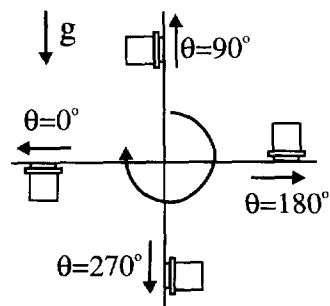
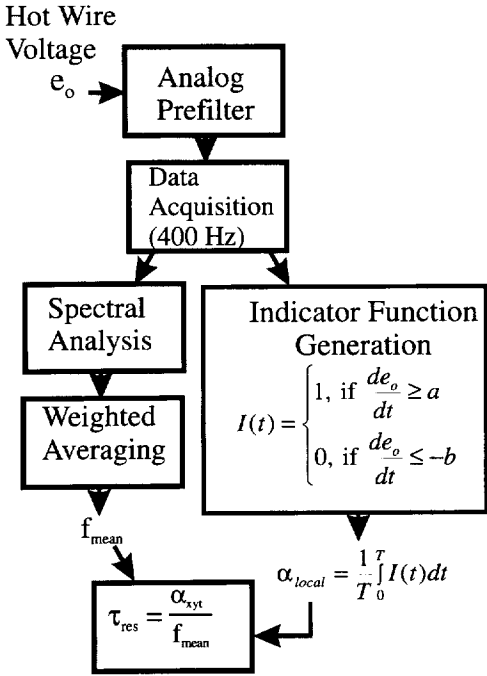Fig. 3. Heater surface orientation designations.

Hot Wire Voltage e_o

Analog Prefilter

Data Acquisition (400 Hz)

Spectral Analysis

Weighted Averaging

f_{mean}

Indicator Function Generation

$$I(t) = \begin{cases} 1, & \text{if } \dfrac{de_o}{dt} \geq a \\[2mm] 0, & \text{if } \dfrac{de_o}{dt} \leq -b \end{cases}$$

$$\alpha_{local} = \frac{1}{T}\int_0^T I(t)\,dt$$

$$\tau_{res} = \frac{\alpha_{xyt}}{f_{mean}}$$

Fig. 4. Flowchart of the hot wire anemometer signal processing sequence.

estimated from a time average of the indicator function. The estimated uncertainty in the peak frequency ranged from about ± 0.2 Hz for heater orientations with a slight angle of inclination relative to $\theta = 180°$ to almost ± 2.0 Hz for the vertical orientation. The uncertainty in the void fraction was estimated at ± 0.04, but was generally higher than that for void fractions of less than about 0.2. The estimated uncertainties in the bubble residence times, calculated from the ratio of the void fraction to the bubble frequency, therefore, ranged from about $\pm 11\%$ for orientations close to 180°, to $\pm 20\%$ for an orientation of 90°.

The mean void fraction is calculated by integrating over the void fraction distribution measured at three different axial locations along the heater surface ($x = 5.1$, 11.5 and 17.8 mm) and at five different heights above the surface ($y = 0.2$, 0.4, 0.8, 1.6, 2.4 and 3.9 mm). The position of the probe was measured in relation to a reference point directly on the heater surface (within ± 0.025 mm), beginning at the leading edge.

The peak bubble frequency is generally more indicative of the behavior of the larger bubbles, since the larger bubbles normally occupy a substantial volume and have diameters far exceeding the length of the sensing wire, increasing the probability for a 'direct hit' on the probe. The smaller bubbles, on the other hand, tend not to produce a defined peak in the spectrum, since they intercept the probe in a more random fashion compared to the larger bubbles, as they may originate from many different sites distributed over the heater surface. So, while the smaller bubbles may be observed as greater in number compared with the

larger ones, the peak frequency is more descriptive of the behavior of the larger bubbles on the heater surface.

EXPERIMENTAL RESULTS

CHF measurements

Figure 5 shows the effect of orientation on the CHF for various subcooling levels with an imposed flow velocity of 0.04 m s^{-1}. At this low flow velocity, the flow forces acting on the vapor are negligible compared with the buoyancy force and, consequently, the CHF values are non-dimensionalized with respect to the correlation by Ivey and Morris [11] for subcooled pool boiling:

$$q_{co} = q_z\left(1 + 0.102\left(\frac{\rho_v}{\rho_l}\right)^{1/4} Ja\right) \tag{1}$$

where q_z is the CHF predicted for pool boiling over an infinite horizontal flat plate by Zuber [3] as

$$q_z = \frac{\pi}{24}\rho_v h_{fg}\sqrt[4]{\frac{g\sigma(\rho_l - \rho_v)}{\rho_v^2}}. \tag{2}$$

Equation (2) is derived assuming a hydrodynamic instability between the vapor and liquid phases, brought about when the kinetic energy of the departing vapor overcomes the stabilizing effect of surface tension at some critical vapor flux corresponding to the CHF. While this expression derived as such gives good agreement with experimental data, it can be alternatively viewed as representing a limit in the rate of latent heat removal allowed by the motion of bubbles liberated from the heat surface through the action of buoyancy. An earlier model of the effects of buoyancy orientation in pool boiling [10] based on the latter criterion is given as follows:

$$q_c = \begin{cases} q_{co}, & 0° < \theta < 90° \\ q_{co}|\sin\theta|^{1/2}, & 90° < \theta < 270° \\ q_{co}, & 270° < \theta < 360° \end{cases} \tag{3}$$

where θ represents the orientation of the heater surface with respect to the buoyancy vector. Equation (3) assumes a buoyancy-driven transport process, thus giving a value of zero for the CHF in the horizontal downward-facing orientation, where the vapor is stagnant. As the angle of inclination increases, the CHF rises accordingly. This is perhaps to be expected in light of the experimental study by Katto and Yokoya [7] of pool boiling with water, in which it was demonstrated that the CHF could be significantly lowered by artificially constraining a bubble on the heater surface to increase its residence time. Hence, the CHF for downward-facing surfaces depends strongly upon orientation angle, as in equation (3) and is nearly zero for $\theta = 180°$, even in the presence of a small imposed flow velocity. For the upward-facing orientations ($0° < \theta < 90°$; $270° < \theta < 360°$), the vapor is able to
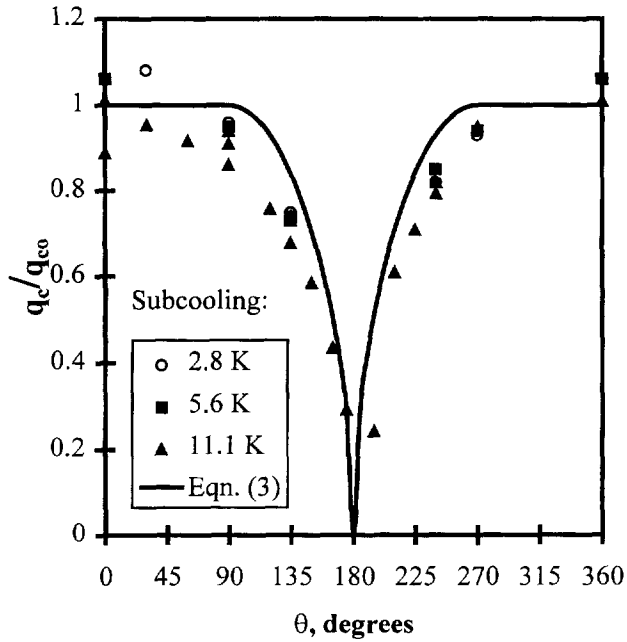
Fig. 5. Measured CHF as a function of heater surface orientation, compared with the CHF model of
equation (3) ; test conditions : $U_{bulk} = 0.04$ m s^{-1} ; $Re = 2700$; $T_{in} = 322$ K.

freely depart the surface and little variation in the
CHF is exhibited. Therefore, while some effect of the
flow inertia is expected for the horizontal facing down
orientation ($\theta = 180°$), the model gives a fair first-
order description of the dependence of the CHF on
orientation at very low flow velocities.

Satisfactory agreement with equation (3) is
obtained in Fig. 5 without the inclusion of a heater
length factor, since the heater length for the present
experiments is roughly equivalent to the most unstable
Taylor wavelength and can, therefore, be considered
to be of 'unit length' at high heat flux. Also note-
worthy is the good correlation of the CHF data by

equation (1) with subcooling for all orientations, sug-
gesting that the basic mechanism through which sub-
cooling raises the CHF is independent of the heater
orientation.

Subcooling effects on the vapor generation rate

Figure 6 shows the volumetric rate of vapor gen-
eration as a function of heater orientation for various
levels of subcooling, estimated from measurements of
the bubble frequency, void fraction and average bub-
ble boundary layer thickness through the following
expression :
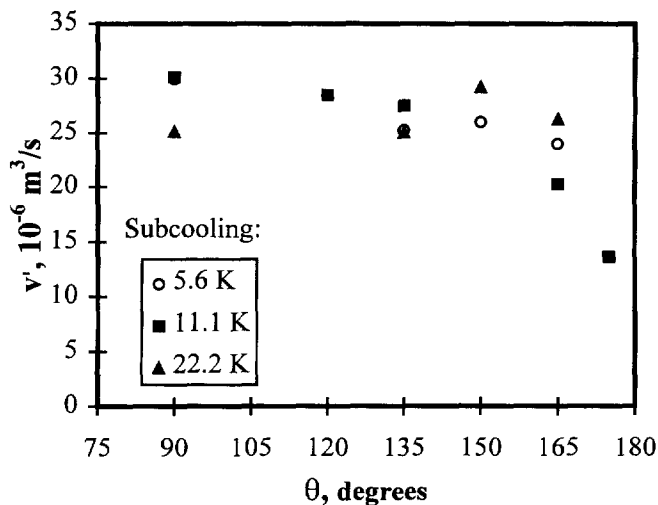
Fig. 6. Volumetric rate of vapor generation as a function of the heater surface orientation for various levels
of subcooling ; test conditions : $U_{bulk} = 0.04$ m s^{-1} ; $Re = 5400$; $T_{in} = 322$ K ; test section height = 25.4
mm.

$$v' = \frac{1}{\tau} w \int_0^L \int_0^\delta \bar{\alpha}_t \, dy \, dx = \bar{f}w(\bar{\alpha}_{xyt}\bar{\delta}_{BBL}L). \qquad (4)$$

Despite the sometimes considerable differences in the CHF brought about by the action of subcooling, the rate of vapor production for each heater orientation remains virtually unchanged. This implies directly that the fraction of the surface heat transfer resulting in evaporation, defined as:

$$\phi \equiv v'/v'_{max} = \frac{v'}{(q_c A_s/\rho_v h_{fg})} \qquad (5)$$

must vary inversely with the subcooling correction factor given for the CHF in equation (1), i.e.:

$$\phi' \equiv \phi\left(1 + 0.102\left(\frac{\rho_v}{\rho_l}\right)^{1/4} Ja\right) = \text{const.} \qquad (6)$$

ϕ' is calculated from Fig. 6 to be about 0.30, varying by about $\pm 20\%$ with the heater orientation. ϕ' tends to be slightly greater for orientations approaching the horizontal down position, where the enhancement in evaporation is likely brought about through the associated increase in the thin film area beneath the flattened, sliding bubbles, as previously observed by Tsung-Chang and Bankoff [12]. However, it is not expected that neglecting such a variation in ϕ' would produce a substantial effect on the bubble growth period, as the equations for bubble growth by Haramura and Katto [1] would indicate.

Typical void fraction distributions measured for $\theta = 150°$ with subcoolings of 5.6 and 11.1 K are shown in Fig. 7. The peak in the void fraction is found to lie at some distance from the heater surface, above the relatively liquid-rich region near the heater surface, which is consistent with the earlier findings by Liaw and Dhir [5] and Iida and Kobayasi [13]. It may also be noted that the void fraction profiles for the three axial locations shown appear to converge to a common value at the heater surface. The void fractions at the heater surface, as extrapolated from the individual void fraction profiles, are given in Fig. 8 for various heater orientations. Generally, the void fractions at the wall lie near values on the order of 0.5, which is close to the predicted maximum packing fraction for a collection of hard spheres, but lower than the values of between 0.68 and 0.80 measured by Liaw and Dhir [5] in pool boiling of water with various contact angles. The values of α_{wall} are extrapolated from locations as close as 0.2 mm to the heater surface, which is generally much smaller than the observed bubble sizes and, therefore, is likely to be adequate enough to characterize the steep change in void fraction.

Two possible mechanisms are responsible for the effects of increasing subcooling on the vapor generation rate exhibited in Fig. 6: (1) the increase in energy required to heat the bulk liquid reaching the surface to the saturated state lowers the rate of vapor generation; or (2) a major fraction of the vapor pro-

duced on the surface is condensed into the bulk liquid. While either mechanism would produce the same effect on v', only the former would yield the effect on the void fraction close to the heater surface shown in Fig. 8. It may, therefore, be inferred that the effect of increasing subcooling is to reduce the rate of evaporation on the heater surface, thereby reinforcing the correlation given by equation (1), which is based on this principle.

Bubble residence time

The mean bubble residence time is estimated from the hot wire measurements by multiplying the mean void fraction by the average time between successive bubbles, given by:

$$\tau^* = \frac{\bar{\alpha}_{xyt}}{\bar{f}}. \qquad (7)$$

The measured bubble residence times then are normalized relative to the value predicted by Haramura and Katto [1] for an infinite horizontal flat plate at CHF, given by:

$$\tau_0^* = \left(\frac{3v'}{4\pi}\right)^{1/5}\left[\frac{4(c\rho_l + \rho_v)}{g(\rho_l - \rho_v)}\right]^{3/5}. \qquad (8)$$

The value of c in equation (8) for an upward facing surface is 11/16, but is approximated here as 0.5, corresponding to the virtual mass of a sphere moving through an infinite medium. A plot of the reciprocal of the normalized residence time at CHF calculated from equation (7) using measurements of $\bar{\alpha}_{xyt}$ and $\bar{f}$ is given in Fig. 9 as a function of orientation. The corresponding measured CHF values are also included, given in dimensionless form relative to the subcooled pool boiling CHF given by equation (1) above. The good correlation between these demonstrates a direct relationship between the CHF and the reciprocal of the bubble residence time, or, equivalently:

$$\frac{q_c \cdot \tau^*}{q_{co} \cdot \tau_0^*} = \text{const.} \qquad (9)$$

at all heater orientations for a given flow velocity and subcooling. This product suggests a mechanism for the CHF which is independent of the orientation with respect to gravity, but associated with the energy per unit area leaving the surface during the bubble residence time. Although the equations and measurements of the bubble residence times given above imply the motion of only a single bubble, the CHF may be considered to be brought about by the global average of the local behavior and the coincidence between the experimental data and equation (9) noted in Fig. 9 stems from the fact that it represents the statistically most probable condition on the heater surface at the CHF.

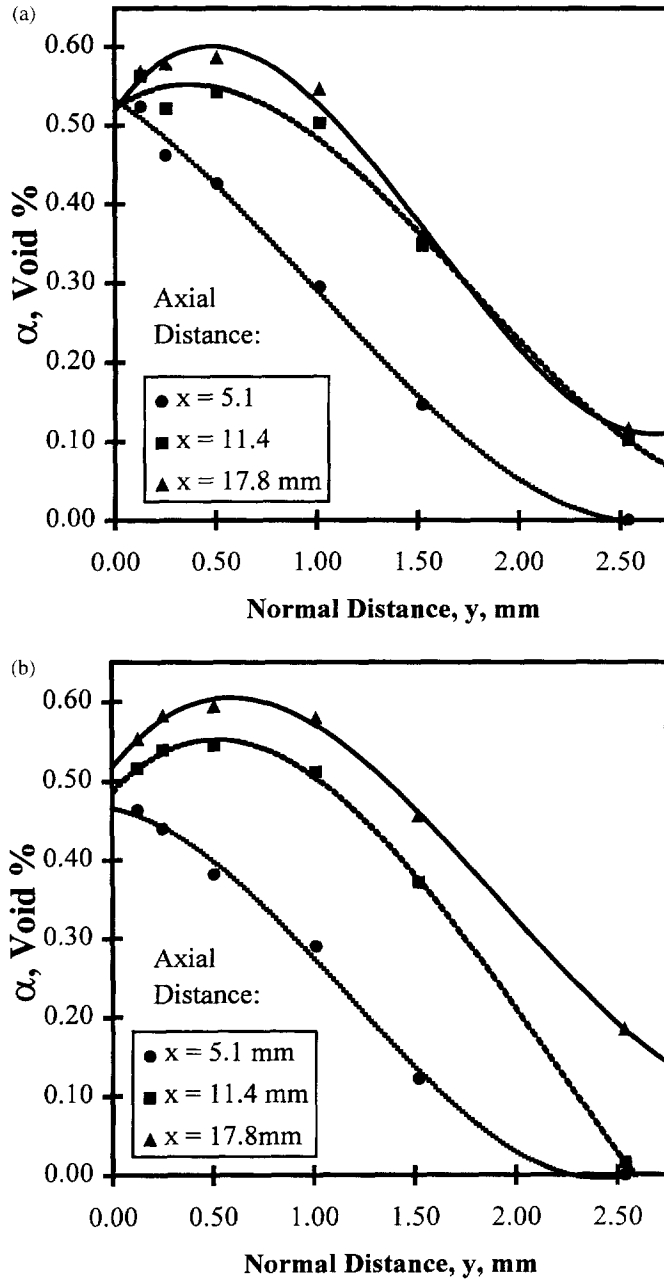Combining equations (1) and (8), the normalizing

Fig. 7. Sample void fraction profiles over the metal heater surface for two different levels of subcooling:
$\theta = 150^\circ$; $U_{bulk} = 0.04$ m s^{-1}; $Re = 5400$; $T_{in} = 322$ K. (a) Void fraction profile at 5.6 K subcooling, q''_w = 150 kW m^{-2}; (b) void fraction profile at 11.1 K subcooling, $q''_w = 175$ kW m^{-2}.

factor for the energy leaving the heater surface at the CHF per unit area is given as:

$$E''_0 \equiv q_c \tau_0^* = q_c \left(\frac{3v'}{4\pi}\right)^{1/5} \left[\frac{4(c\rho_1 + \rho_v)}{g(\rho_1 - \rho_v)}\right]^{3/5} \quad (10)$$

where v' can be evaluated from experimental data in Fig. 6. The energy per unit area leaving the heater surface during the bubble residence time at some heat flux level below the CHF, meanwhile, can be denoted as

$$E''_s = q_s \cdot \tau_{res}. \quad (11)$$

The measured values of E''_s normalized with respect to equation (11) are given in Fig. 10 as a function of the surface heat flux normalized with respect to the measured CHF, for heat flux levels ranging from about 50–95% of CHF. The measurements are compared with a model for bubble growth at high heat fluxes given by Haramura and Katto [1], assumed here to apply to heat flux levels below the CHF, given by:
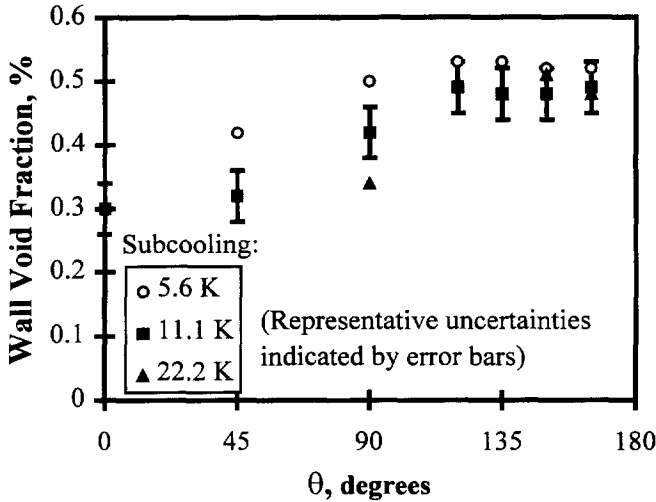
Fig. 8. Measured void fraction extrapolated to the heater surface as a function of heater surface orientation for various levels of subcooling; test conditions: $U_{bulk} = 0.04$ m s^{-1}; $Re = 5400$; $T_{in} = 322$ K; test section height $= 25.4$ mm.
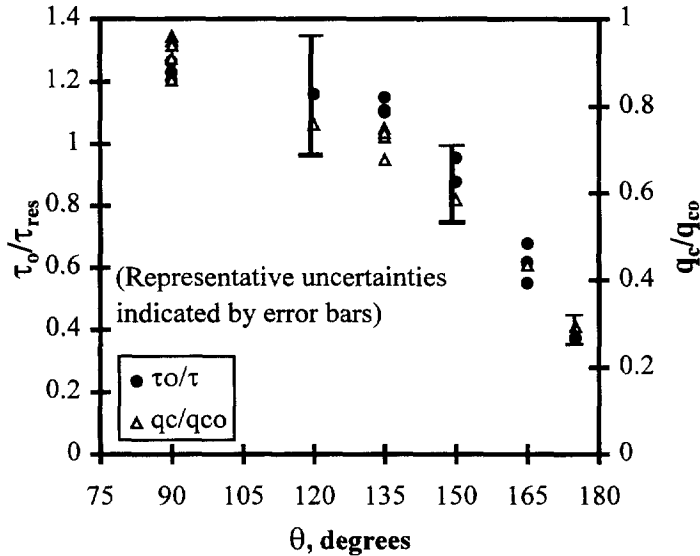
Fig. 9. Reciprocal of the measured bubble residence time as a function of heater surface orientation compared with the corresponding CHF; test conditions: $U_{bulk} = 0.04$ m s^{-1}; $Re = 5400$; $T_{in} = 322$ K; test section height $= 25.4$ mm.

$$E_s''|_{theor} \equiv q_s \tau_{res} = q_s \left(\frac{3}{4\pi} \phi' \frac{q_s A_s}{\rho_v h_{fg}}\right)^{1/5} \left[\frac{4(c\rho_1 + \rho_v)}{g(\rho_1 - \rho_v)}\right]^{3/5}.$$

(12)

The trends in the relationship between E_s'' and q_s/q_c shown for the various heater orientations and sub-coolings in Fig. 10 show reasonable qualitative agreement with equation (12), indicating that the physics of the bubble growth and motion described by the model are essentially incorporated for this range of heat flux. The quantitative discrepancies between the measured and predicted values, however, may demonstrate that the equations derived considering only

an isolated bubble do not apply exactly to a group of bubbles growing in proximity to one other on the heater surface. The increase in E_s'' as the orientation angle approaches the horizontal down position, seen most prominently for $\theta = 165°$, presumably is associated with the flattening of the bubbles, which would increase the latent heat transport fraction in equation (5), increasing somewhat the total energy transport needed to trigger the CHF.

Visual observations using high-speed photography

A typical bubble lifetime at high heat flux is shown in Fig. 11 at 12 ms intervals during its growth and
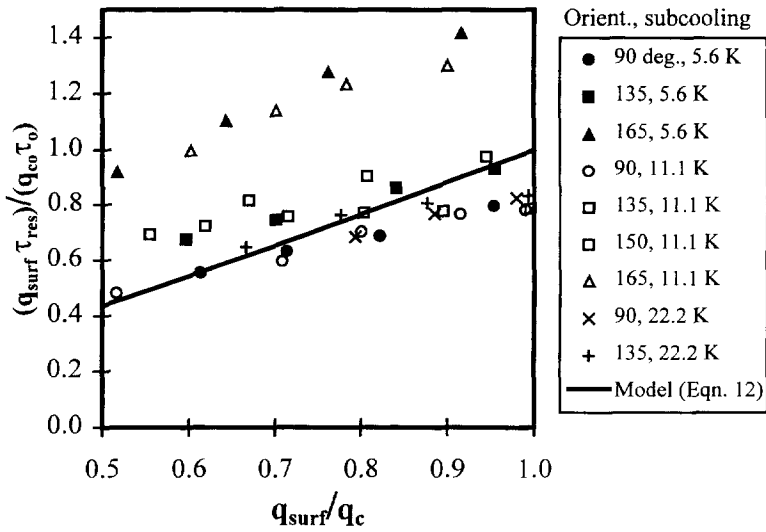
Fig. 10. Relationship between the product of the surface heat flux and the bubble residence time as a function of the surface heat flux, shown in nondimensional form for various heater surface orientations ranging from 90 to 165° and bulk liquid subcoolings ranging from 5.5 to 22.2 K; $U_{bulk} = 0.04$ m s^{-1}; $Re = 5400$; $T_{in} = 322$ K; test section height = 25.4 mm.
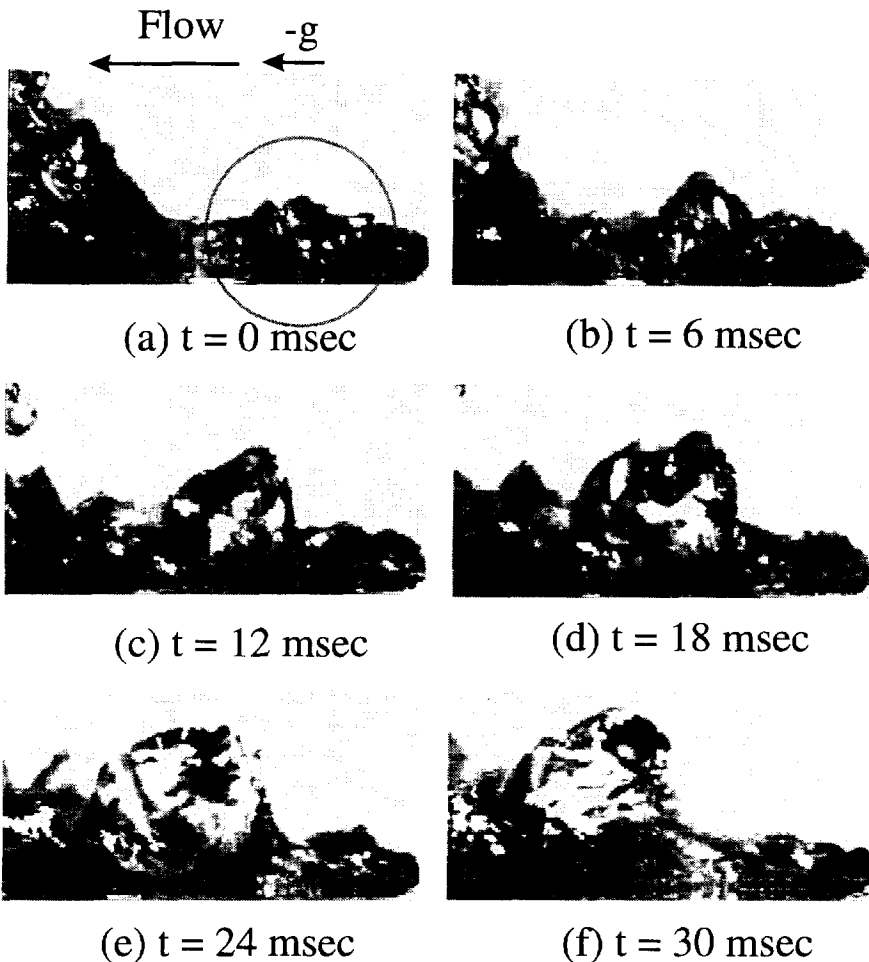

Fig. 11. A typical large bubble shown at 6 ms intervals during its growth and departure cycle (side view of a metal heater surface): $\theta = 90°$; $q'' = 300$ KW m^{-2}; $U_{bulk} = 0.08$ m s^{-1}; $\Delta T_{sub} = 11.1$ K; $T_{in} = 322$ K.

departure cycle. The photographs show the side view of a relatively large bubble growing on the metal heater surface in the vertical upflow orientation ($\theta = 90°$) at 11.1 K subcooling. The first frame identifies the bubble in its earlier stages of growth, where it appears to originate from the coalescence of a cluster of smaller bubbles. As time progresses, the bubble grows and accelerates along the heater surface due to buoyancy. From high-speed photographs viewed normal to the heater surface (not shown in the figure), using the heater length as a reference, the larger bubble sizes are estimated to be an average of between 6 and 8 mm in diameter. The photographs give no evidence of vapor stems at the base of the growing bubbles, nor of a Kelvin–Helmholtz instability between the liquid and vapor. Nevertheless, these larger bubbles would appear to take on a significant role in the mechanisms of dryout by virtue of the heater surface area they occupy.

Figure 12 shows boiling at 10 ms intervals during a single growth and departure cycle on the gold film heater at heat flux levels approaching the CHF, viewed through the heater surface from below, for $\theta = 135°$ and $\Delta T_{sub} = 11.1$ K. While the thermal properties of the quartz substrate are such that the CHF occurs at a lower level than for the copper block heater, the heat flux nonetheless exceeds the first hydrodynamic transition level of Moissis and Berenson [14], marking the change from individual bubbles to the coalesced vapor mushrooms described by Gaertner [9]. No vapor stems are observed beneath the bubbles here and the dryout (indicated by the nearly white areas beneath the bubbles) appears to be a localized phenomenon occurring in patches on the surface, as was previously seen in the photographs of Kirby and Westwater [6]. While the vapor stem model is purported to be valid for downward-facing surfaces as well as upward-facing ones, the photographs in Figs
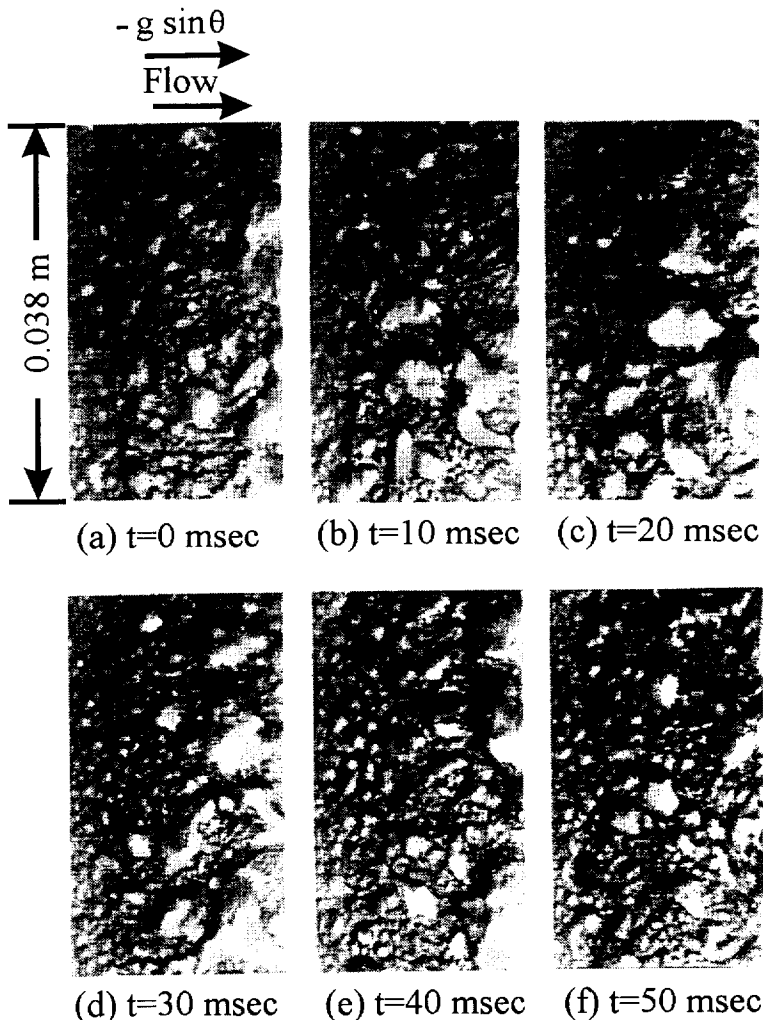

Fig. 12. Sequential photographs of boiling of R-113 on a gold film heater viewed from below during a complete growth and departure cycle: $\theta = 135°$; $q'' = 136$ kW m^{-2}; $U_{bulk} = 0.04$ m s^{-1}; $\Delta T_{sub} = 11.1$ K ; $T_{in} = 322$ K.

11 and 12 provide no evidence to support the existence of such vapor stems, nor of any uniform liquid macrolayer.

DISCUSSION

The experimental data here show the macrolayer and vapor stem models to be accurate in many respects, but inconsistent mainly in their description of the evaporation process. The data presented in Figs. 9 and 10 suggests the validity of the kinematic expressions for the growth and motion of vapor bubbles used by Haramura and Katto [1]. At the same time, the structure dictated by the macrolayer and vapor stem models appears physically inaccurate, though they have been used to accurately characterize many important experimentally-observed phenomena, such as dry spot formation and the CHF. The vaporization energy per unit area in the macrolayer, given by the product of the CHF and bubble residence time, seems to be constant for all heater orientations, as noted in Fig. 9. This quantity, denoted by E'', by itself implies no definite structure for the evaporating regions on the heater surface and in this sense is a weaker modeling tool than the macrolayer concept. Yet, the photographic evidence given here, particularly in Fig. 12, suggests the macrolayer to be physically inaccurate, leaving E'' as a more general concept that can be sustained by experimental evidence.

The data of E'' for increasing heat flux levels in Fig. 10 points to the validity of using a balance of virtual mass acceleration and buoyancy forces to approximate the motion of a growing bubble. While Kumada and Sakashita [8] observed the presence of many different bubble sizes at high levels of heat flux, the success of this first-order model further suggests the primary importance of the motion of the large bubbles in determining the CHF. The significance of the larger bubbles arises from their role in the formation of dry spots on the heater surface, which Ishigai and Kuno [15] showed appear periodically on the heater surface with increasing size and frequency at increasingly high levels of heat flux. Figure 10 also serves to demonstrate another important point, that E' reaches a maximum value at the CHF that its nearly constant for all heater orientations.

The energy per unit area E'' can be viewed as being analogous to the macrolayer, since the assumption of a uniform and constant macrolayer thickness for the various orientations, though physically unrealistic, nonetheless implies the same concept. The existence of a macrolayer isolated from the bulk liquid region by a vapor barrier, on the other hand, dictates that all of the energy leaves the heater surface by evaporation. While such a hypothesis has a precedent in many early studies of latent heat transport [16], the measurements of the vapor generation rate for R113 given in Fig. 6 indicate that only about one quarter of the total heat flux accounts for the growth rate of the large bubbles.

Indeed, were all of the energy leaving the heater surface to go into the formation of the large bubbles, the equations for bubble growth used by Haramura and Katto [1] in the macrolayer dryout model would predict bubble departure diameters of nearly 80 mm for water and 13 mm for R113. Both experimental measurements of bubble sizes for water [17] and high speed photographs of departing bubbles, such as those given in Fig. 11 for R113 and by Gaertner [9] for water, show this to be a gross over-prediction. Instead, evaporation appears to be confined to localized regions on the heater surface beneath growing bubbles, as in the photographs in Fig. 12 of boiling viewed from below, with no evaporation over the greater portion of the heater surface. Together with the measured volumetric vapor generation rates in Fig. 6, this evidence suggests that heat transfer modes other than latent heat transport, normally considered to be negligible, contribute significantly to the process.

The net effect of subcooling in increasing the CHF, demonstrated in Fig. 5, is consistent with the Ivey and Morris [11] correlation for pool boiling. The reduction in the volumetric rate of vapor generation with increasing subcooling demonstrated in Fig. 6 is somewhat different from that which has been assumed in earlier models, particularly those which describe the CHF in terms of a hydrodynamic instability. In such models, the Kelvin–Helmholtz instability between the liquid and vapor occurs at some critical vapor velocity. The velocity of the vapor leaving the surface, considering strictly latent heat transport from the heater surface is then given from continuity as:

$$U_v = \frac{q_s A_s}{\rho_v h_{fg} A_v} \qquad (13)$$

where A_v is the area occupied by vapor stems and A_s is the total heater surface area. In subcooled pool boiling, where the CHF may be increased substantially, such an assumption requires either that the net vapor velocity be decreased by condensation into the bulk liquid [18], or that the vapor stem diameter increase substantially with subcooling. However, neither premise can be substantiated by experimental observations and correlations based on condensation into the bulk liquid generally compare unsatisfactorily with experimental data. Therefore, assuming a hydrodynamic instability mechanism for subcooled pool boiling necessitates that the equivalent of the latent heat fraction parameter of equation (6) be introduced for consistency.

In summary, the experimental results of this work suggest that existing CHF models for pool boiling accurately describe the growth and motion of bubbles at high levels of heat flux, but that the physical description of the evaporation on the heater surface could be improved. The energy per unit area leaving the heater during the bubble residence time, E'', represents an alternative to the macrolayer and to the assumption that all heat is transferred from the surface by evap-

oration. A new model for subcooled, low-velocity forced convection boiling is presented in the second part of this work, which successfully correlates the results obtained in the present experimental study.

CONCLUSIONS

From the experimental results for low-velocity forced convection boiling presented here, it is concluded that:

(1) An inverse relation exists between the bubble residence time and the CHF, suggesting that the product of the CHF and the bubble residence time, representing the energy per unit area leaving the heater surface during the bubble residence time, is independent of changes in the orientation of gravity.

(2) The growth and motion of large bubbles at heat flux levels approaching the CHF are modeled reasonably well by a balance of buoyancy and virtual mass forces acting on a spherical bubble growing with a constant volumetric generation rate.

(3) Subcooling increases the CHF while also lowering the rate of vapor generation on the heater surface. The increase in the CHF with subcooling correlates with Ivey and Morris [11] expression for pool boiling, while measurements with R113 show that evaporation accounts for only about one third of the total heat flux at CHF, even for the saturated case.

(4) Evaporation and dryout appear to occur in highly localized regions on the heater surface beneath growing bubbles.

The first conclusion above suggests a mechanism for the CHF common to all heater orientations and is basically equivalent to the dryout mechanism assumed in the macrolayer dryout models. While the second conclusion suggests the validity of the bubble dynamics assumed in the macrolayer dryout models, the third and fourth suggest substantial areas for improvement in the description of the evaporative regions on the heater surface, currently represented by vapor stems and an isolated liquid macrolayer. A semi-empirical model for the evaporation process is proposed in the companion work, which is consistent with these experimental conclusions.

REFERENCES

1. Haramura, Y. and Katto, Y., A new hydrodynamic model of critical heat flux, applicable to both pool and forced convection on submerged bodies in saturated liquids. *International Journal of Heat and Mass Transfer*, 1983, **26**, 389–399.
2. Pasamehmetoglu, K. O., Chappidi, P. R., Unal, C. and Nelson, R. A., Saturated pool nucleate boiling mechanisms at high heat fluxes. *International Journal of Heat and Mass Transfer*, 1993, **36**, 3859–3868.
3. Zuber, N., On the stability of boiling heat transfer. *Transactions of the ASME, Series C, Journal of Heat Transfer*, 1958, **80** (4), 711–720.
4. Lienhard, J. H. and Dhir, V. K., Hydrodynamic prediction of peak pool-boiling heat fluxes from finite bodies. *Transactions of the ASME, Series C, Journal of Heat Transfer*, 1973, **95** (2), 152–158.
5. Liaw, S. P. and Dhir, V. K., Void fraction measurements during saturated pool boiling of water on partially wetted vertical surfaces. *Transactions of the ASME, Journal of Heat Transfer*, 1989, **111** (3), 731–738.
6. Kirby, D. B. and Westwater, J. W., Bubble and vapor behavior on a heated horizontal plate during pool boiling near burnout. *Chemical Engineering Progress Symposium Series, Heat Transfer*, 1965, 238–248.
7. Katto, Y. and Yokoya, K., Principal mechanism of boiling crisis in pool boiling. *International Journal of Heat and Mass Transfer*, 1968, **11**, 993–1002.
8. Kumada, T. and Sakashita, H., Pool boiling heat transfer—II. Thickness of liquid macrolayer formed beneath vapor masses. *International Journal of Heat and Mass Transfer*, 1995, **38**, 979–987.
9. Gaertner, R. F., Photographic study of nucleate pool boiling on a horizontal surface. *Transactions of the ASME, Series C, Journal of Heat Transfer*, 1965, **88** (1), 17–29.
10. Brusstar, M. J. and Merte, H., Jr, Effects of buoyancy on the critical heat flux in forced convection. *AIAA Journal of Thermophysical Heat Transfer*, 1994, **8** (2), 322–328.
11. Ivey, H. J. and Morris, D. J., On the relevance of the vapor–liquid exchange mechanism for subcooled boiling heat transfer at high pressure. UKAEA, AEEW-R 137, 1962.
12. Tsung-Chang, G. and Bankoff, S. G., On the mechanism of forced-convection subcooled nucleate boiling. *Transactions of the ASME, Journal of Heat Transfer*, 1990, **112** (1), 213–218.
13. Iida, Y. and Kobayasi, K., Distributions of void fraction above a horizontal heating surface in pool boiling. *Bulletin of the JSME*, 1969, **12** (50), 283–290.
14. Moissis, R. and Berenson, P. J., On the hydrodynamic transitions in nucleate boiling. *Transactions of the ASME, Journal of Heat Transfer*, 1963, **85** (3), 351–358.
15. Ishigai, S. and Kuno, T., Experimental study of transition boiling on a vertical wall in open vessel. *Bulletin of the JSME*, 1966, **9** (34), 361–368.
16. Bankoff, S. G., A note on latent heat transport in nucleate boiling. *A. I. Ch. E. Journal*, 1962, **8** (1), 63–65.
17. McFadden, P. W. and Grassman, P., The relation between bubble frequency and diameter during nucleate pool boiling. *International Journal of Heat and Mass Transfer*, 1962, **5**, 169–173.
18. Zuber, N., Tribus, M. and Westwater, W., The hydrodynamic crisis in pool boiling of saturated and subcooled liquids. *International Developments in Heat Transfer: Proceedings of the 1961 Heat Transfer Conference*, Paper 27. ASME, New York, 1961, pp. 230–236.